Nanorobotics | Hot Paper

Tunable Release of Multiplex Biochemicals by Plasmonically Active Rotary Nanomotors**

Xiaobin Xu, Kwanoh Kim, and Donglei Fan

Abstract: *It is highly desirable to precisely tune the molecule release rate from the surfaces of nanoparticles (NPs) that are relevant to cancer therapy and single-cell biology. An innovative mechanism is reported to actively tune the biochemical release rate by rotation of NPs. Plasmonic nanomotors were assembled from NPs and applied in multiplex biochemical release and detection. Both single and multiplex biosignals can be released in a tunable fashion by controlling the rotation speed of the nanomotors. The chemistry and release rate of individual chemicals can be revealed by Raman spectroscopy. The fundamental mechanism was modeled quantitatively and attributed to the fluidic boundary-layer reduction owing to the liquid convection. This work, which explored the synergistic attributes of surface enhanced Raman scattering and nano-electromechanical systems, could inspire new sensors that are potentially interesting for various bio-applications.*

The great potential of nanoparticles for biosubstance delivery has led to considerable research interest owing to their controllable geometry, chemistry, and surface functionality.[1] Various nanoentities were explored for in vivo drug delivery and cancer therapy.[1,2] Among them, one-dimensional nanoentities, such as nanowires and nanotubes, received special attention, the lengths and diameters of which could be controlled to the scales of live cells and biomolecules, respectively.[3] They were applied as vehicles for transporting biospecies, such as cytokines,[4] peptides,[5] enzymes,[6] and genes,[7] for in vitro stimulation.[4] Nevertheless, it remains a grand challenge to release biosubstances attached on nanoparticles in a tunable fashion, the feast of which could enable an in-depth understanding of the fundamental sciences in drug delivery, single cell stimulation, and cell–cell communication.[4]

Previously, pulsed electric potentials were employed to release biosubstances from patterned microelectrodes,[8]

[*]   X. Xu, Prof. Dr. D. L. Fan
      Materials Science and Engineering Program
      Texas Materials Institute, The University of Texas at Austin
      Austin, TX 78712 (USA)
      E-mail: dfan@austin.utexas.edu

      K. Kim, Prof. Dr. D. L. Fan
      Mechanical Engineering, The University of Texas at Austin
      Austin, TX 78712 (USA)

demonstrating the feasibility of electrically induced biochemical release from nanoparticles. However, this intriguing mechanism requires complex lithographical patterning to electrically connect nanoparticles. Recently, heat generated from optical excitation of plasmonic nanoparticles was used for releasing gene molecules.[9] Vibrations induced by the radio-frequency electromagnetic fields were also used to enhance the releasing rate of drug molecules.[10] Recently, self-propelled nanomotors were used to actively release desired ions.[11] Acoustically driven nanomotors were actuated inside live cells.[12] Nevertheless, it remains a daunting task to tune the molecular release rate from individual nanoparticles with high precision while simultaneously monitoring.

Recently, we reported an innovative type of electrically driven nanomotors assembled from nanoscale building blocks with ultrahigh speed and fixed rotation positions. A preliminary study demonstrated the controlled release of biochemicals from such nanomotors.[13] However, a systematic study has not been conducted, which is highly desirable to understand the fundamental mechanism. It is also of great interest to release more than one type of molecules from the nanomotors.

In this research, we systematically investigated the concept of motorization of plasmonic nanosensors for tuning the release rate of biochemicals, their real-time detection, and the underline mechanism by experimentation and analytical modeling. The nanomotors, with enhanced functionalities in both molecular sensing and actuation, were assembled from designed plasmonic nanoparticles and patterned nanomagnets, and rotated with controlled speed and chirality by electric tweezers.[14] Both single and multiple analytes can be released in a tunable fashion by the mechanical rotation of the nanomotors. The chemistry and concentration of individual analytes were revealed simultaneously by using high-speed micro-Raman spectroscopy. The fundamental mechanism was investigated and attributed to the convection induced fluidic boundary-layer reduction, which quantitatively agrees with the experimental results. To the best of our knowledge, this effect is observed and understood in the micro/nanomechanical system for the first time. This research, exploring robotized nanomotor sensors by integrating SERS[3,15] and NEMS, could be of interest for biologically relevant applications.[4,12,16]

The designed nanomotor system consists of plasmonically sensitive nanorod as rotors, patterned nanomagnets as bearings, and microelectrodes as stators (Figure 1a). The plasmonic naonrotor, the most critical component of a nanomotor for attaching and detecting biochemicals, has a three-layer structure with a core made of a Au/Ni/Au three-segment
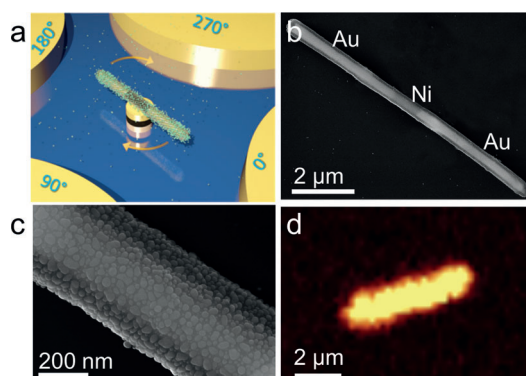
Figure 1. a) Representation of a rotating nanomotor sensor that releases molecules. b) Scanning electron microscopy (SEM) images of a plasmonic nanorod for the nanomotor rotor made of a three-layer structure with a Au-Ni-Au nanowire as the core, a silica coating, and a dense layer of Ag nanoparticles on the outer surface of silica. c) A higher-magnification SEM image shows the dense Ag nanoparticles grown on the silica. d) Raman mapping of 1 μм R6G dispersed on a plasmonic nanomotor rotor showing essentially uniform SERS intensity on the surface.

nanowire, a layer of silica conformably coated on the nanowire core, and uniformly surface-distributed Ag nanoparticles (NPs) synthesized on the outer surface of silica (Figure 1a). Here, each layer of the plasmonic nanorotor was designed to serve a purpose: the metallic nanowire core can be efficiently polarized in electric fields for fast transport and rotation by our recent invention (the electric tweezers);[14] the Ni segment presented in the nanowire core assists the anchorage of the plasmonic nanorotor on a pre-patterned nanomagnet into a nanomotor;[13] and the mesoporous silica coating with densely surface-distributed AgNPs (ca. 1570 μm^2) provides efficient absorption of molecules and their ultrasensitive Raman detection.[17] It is worth noting that this shows that AgNPs are biocompatible when their concentration is below a certain threshhold, suggesting a window for the biological application of AgNPs.[18] AuNPs could be more advantageous in terms of a higher biocompatibility, while the Raman enhancement effect of which is generally lower than that of AgNPs in the visiable regime.[19]

Three steps were taken to fabricate the plasmonic rotors. In brief, the multi-segment Au/Ni/Au nanowires (300 nm in diameter) were synthesized by electrodeposition into nanoporous templates[14a, 20] before a 70 nm-thick silica layer was evenly coated on the outer surface of nanowires by the hydrolysis of tetraethyl orthosilicate.[21] Next, a large array of AgNPs were synthesized uniformly on the surface of silica in a mixture of silver nitrite and ammonia catalyzed by polyvinylpyrrolidone (PVP) for 7 h at 70 °C.[21] Finally, the as-synthesized nanowire rotors were sonicated, centrifuged, and washed before redispersed in deionized (DI) water. The experimental details are provided in the Supporting Information.

Scanning electron microscopy (SEM) confirmed the successful synthesis of the three-layered plasmonic rotors (Figure 1b,c). The AgNPs, densely distributed on the rotor

surfaces, were semi-spherical, with an average diameter of 25.2 ± 6.4 nm and density of about 570 μm^2. If considering the NP junctions of less than 2 nm as the plasmonic hotspots, where Raman signals of molecules can be substantially enhanced owing to ultrahigh electric fields generated by the coherence oscillation of conduction-band electrons,[22] we found the density of hotspots can be as high as about 1300 μm^2. These hotspots are distributed along the plasmonic nanorotor essentially uniformly as shown in the Raman mapping of Rhodamine-6G (R6G) molecules (Figure 1d, 1 μм R6G incubated with the plasmonic nanorotor for 2 h before being dried). The Raman image was taken from a single plasmonic nanorotor by using a confocal Raman microscope exciting at 532 nm with a step size of 250 nm and a spot size of about 1 μm. The integration time of each spectrum was set at 0.5 s. The Raman enhancement factor of such kind of plasmonic nanorotors can be estimated as being about 10^{10} following a method reported previously,[23] one of the highest among the state-of-the-art.[24] In the control experiment, we did SERS characterization of Nile Blue (NB) (340 nм) from a nanorod without AgNPs, that is, a silica-coated Au-Ni-Au nanorod. No NB signal can be detected (Supporting Information, Figure S2).

The strong Raman enhancement and high density of hotspots on the plasmonic nanorotors are pivotal for ultrasensitive SERS detection.[3,15b] Using them, we can readily determine both the chemistry and concentration of multiple molecules simultaneously with Raman spectroscopy. NB and R6G, two commonly used SERS probes, were employed for demonstration purposes owing to their large Raman scattering cross-sections and wide biological applications.[25] A series of R6G and NB in DI water suspension were incubated with the plasmonic nanorotors for 30 min. Then the Raman spectra were collected by using a Raman microscope equipped with 532 and 632.8 nm lasers. It was shown that the Raman intensity monotonically increased with the concentration of NB (or R6G), from which the concentrations of analytes can be quantitatively determined (Supporting Information, Figure S1a–e). Note that we measured multiple plasmonic nanorotors deposited on the substrate to obtain the average of Raman intensity for each concentration. The detection is highly sensitive that the time-dependent absorption of biomolecules (NB, 50 nм) to their surfaces can be monitored, which shows a monotonic increase before reaching a saturation plateau at about 70 s (Supporting Information, Figure S1f).

More importantly, the structure of the plasmonic nanorotor was carefully designed for robotization. The nanomotors consist of the plasmonic nanorods serving as nanomotor rotors and patterned nanomagnets as bearings (a thin film stack of Au (100 nm)/Ni (80 nm)/Cr (6 nm), 1 μm in diameter; Figure 1a). To assemble such nanomotors, we employed the electric tweezers, a recently developed nanomanipulation technique that can align and transport nonspherical nanoentities with a precision of at least 300 nm.[14a,26] The randomly suspended plasmonic nanorotors were manipulated in both the X and Y directions. The transport velocity increased linearly with the applied DC voltages (Figure 2a). When the plasmonic nanorotors were in the vicinity of the
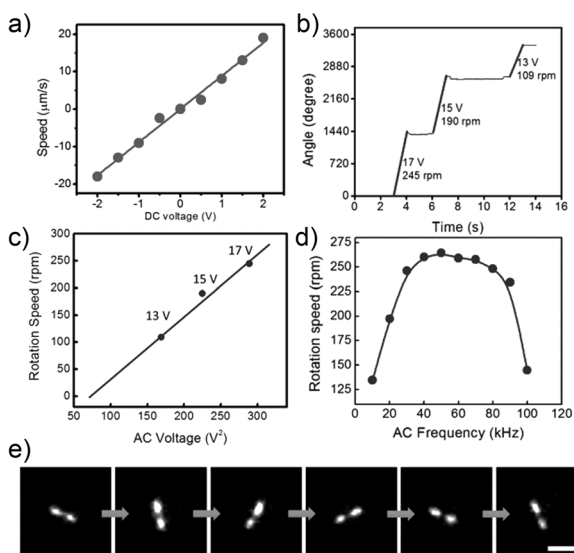
Figure 2. a) The transport speed of the plasmonic nanorotor, which increases with the applied DC voltage. b),c) The rotation speed of nanomotor sensors, which increases linearly with V^2 (20 kHz) and d) depends on the applied AC frequency (15 V). e) Snapshots (every 1/6 second) of a rotating nanomotor functionalized with NB imaged in the Raman mode. Note that the objective of the inverted microscope is underneath the rotating nanomotor. Thus the Raman image of the middle of the plasmonic nanomotor was blocked by the magnetic bearing. Scale bar: 10 μm.

nanomagnets, they were swiftly attracted and assembled on the nanomagnets owing to the magnetic attraction. Then, a rotating electric field was generated by four AC electric voltages with sequential 90° phase-shift applied to the quadrupole microelectrodes, which compelled the assembled nanomotors into rotation (Figure 1a, Figure 2b; Supporting Information, Video S1).

The rotation is a result of the induced electric torque (T_e) generated from the interactions between the polarized plasmonic nanorotors and the external AC electric field,[14b,27] where $T_e \approx E^2$. The E^2 dependence of the rotation speed (ω) accounts for the V^2 dependence in Figure 2c. Along with the applied voltage, the speed of the nanomotor sensors can also be optimized by the applied AC frequency, where the highest value obtained at 50 kHz in the range of 10 to 100 kHz (Figure 2d). As a result, the nanomotor sensors can be successfully synthesized, assembled, and actuated with high sensitivity for biochemical detection and controllability in mechanical rotation.

Next, we investigated the applications of nanomotors for tuning the biochemical release and the involved fundamental mechanisms. Both the releases of single (NB) and multiplex biochemicals (mixture of NB and R6G) were studied. The molecules were functionalized on the surface of the plasmonic nanorotors by incubation followed by redispersion in DI water (Supporting Information). Immediately after the dispersion, the plasmonic nanorotors were quickly assembled into nanomotors and rotated (Supporting Information, Video S1). The distribution of molecules on the surface of nanomotors can also be directly imaged and videotaped detected by the ultrasensitive high-speed CCD camera at

a frame rate of 24 fs^{-1} from their Raman images (Figure 2e; Supporting Information, Video S2). In the study of molecule release of NB, the rotation speed of nanomotors was precisely controlled from 195 rpm to 75 rpm at 17 to 10 V (Supporting Information, Video S3). The molecule release rate from the surface of the rotating nanomotor was monitored and recorded simultaneously by using high-speed Raman spectroscopy operating at 0.5 spectrum per second (Figure 3a,b).
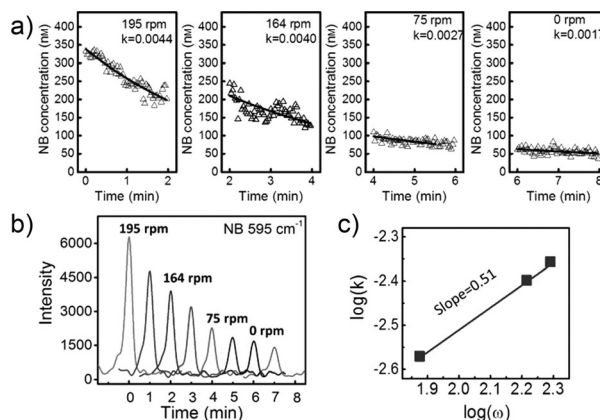

Figure 3. Tunable release of biochemical by the mechanical rotation of nanomotor sensors. a) Concentration of NB versus time at different rotation speeds. b) Representative Raman spectra of R6G every 1 min at each rotation speed. c) The release rate, which monotonically increases with the rotation speed with a power-law dependence of 0.51.

The release of molecules (340 nM NB) from the surface of a rotating nanomotor (126 rpm) can be detected for a long duration, for example, 30 min (Supporting Information, Figure S4). The molecule release from a static nanomotor is also shown in the Supporting Information, Figure S5.

It was found that, regardless of the rotation speed or the molecular species, the concentration of molecules measured with the Raman spectroscopy decreases with time monotonically. Note that only those molecules attached on the surface of the nanomotor sensors can be detected, which is due to the significant plasmonic enhancement from the AgNPs. The molecular concentration on the surface of nanomotors was also much higher than that in the bulk solution. As a result, a net molecular mass flow can be established from the nanomotor sensors to the bulk solution, consistent with the monotonic concentration decrease as observed in the Raman spectroscopy.

This phenomenon can be modeled by using the Nernst diffusion-layer theory, which is widely used to understand phenomena involving solid–liquid interfaces.[28] According to this theory, at the interface of a solid surface and a suspension medium, a stationary liquid layer is formed with a thickness of λ. Within such a stationary layer, the transport of mass between the solid surface and bulk liquid, such as molecules or ions, can only occur by the passive diffusion in the direction of the chemical gradient. Out of such a region, liquid convection dominates, which can actively pump molecules to the outer boundary of the stationary layer. If the concen-
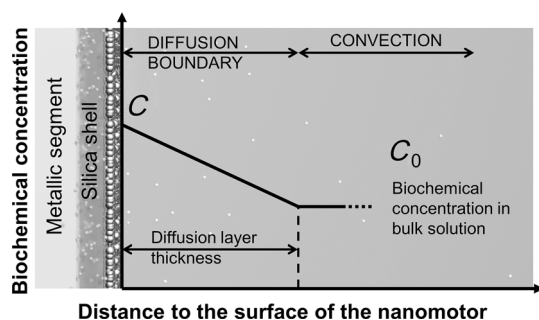
Figure 4. Diagram of the model of the diffusion boundary layer next to the surface of the nanomotor sensors. Small spheres: biochemical molecules; large spheres: Ag NPs.

tration of the analyte molecules at the layer boundary is approximated to be the same as that in the bulk solution, a static concentration gradient can be established across this stationary diffusion layer (Figure 4). According to the Fick's diffusion laws, the time dependent concentration of molecules on the surface of nanomotors (C) can be calculated as:

$$C = C' e^{-kt} + C_0 \qquad (1)$$

where $C' = C_1 - C_0$, C_1 is the initial concentrations of NB on the surface of nanomotors, C_0 is the concentration of NB in the bulk solution, and k (s^{-1}) is the molecule release rate. The value of k is proportional to D/λ, where D is the diffusion coefficient of the NB molecules. From Equation (1), we can readily determine the rate of molecule release when the nanomotor sensors were rotated at different speeds (ω). Here, at each rotation speed, the data points was fitted according to Equation (1) by using Origin software with the initial C_1 given as the as-measured values (Figure 3 a,b). Interestingly, the molecule release rate k monotonically increased with the rotation speed with a power-law dependence of $k \propto \omega^{0.51}$ (Figure 3 c). It is highly desirable to understand the governing mechanism of such a relation. We attribute the mechanism to the stationary diffusion layer reduction as a result of the liquid convection owing to the rotation of nanomotors. According to the classical boundary layer theory,[29] a flow with a speed of v passing on a flat surface can result in the thinning of the stationary layer next to the solid surface owing to fluidic convection promoted by the flow, whereas the thickness of the stationary layer follows the relation of $\lambda \propto R_e^{-0.5} \propto v^{-0.5}$.[29] Given the molecular release rate of $k \propto D/\lambda \propto 1/\lambda$ and the fluidic velocity (v) proportional to the rotation speed (ω) of nanomotor sensors ($v \propto \omega$), it can be readily known that $k \propto \sqrt{\omega}$, which quantitatively agrees with our experimental observation of $k \propto \omega^{0.51}$ (Figure 3 c). Moreover, we note that the theory for the rotating disk electrode (RDE) system, studied extensively by electrochemistry,[28] further supports our understanding, which indicates that the transport of ionic masses to a rotating disk electrode increases with the rotation speed of the electrode with a power-law dependence of 0.5.[28,30]

It is also important to know whether the applied AC electric (E) fields could directly alter the molecule release rate.[27b] A control experiment was performed on a stationary

nanomotor functionalized with NB molecules. The AC rotating E fields (17 V, 20 kHz) were turned on and off alternately for multiple times, while the molecular release was monitored simultaneously. The molecular release rate remained unchanged when the E field was either on or off, which suggests that the AC E field has negligible effect on molecule release rate (Supporting Information, Figure S3). This experiment was repeated many times to confirm the observation.

The next question is whether the above mechanism is applicable to the release of multiplex biochemicals. To address this question, we functionalized the nanomotor sensors with a mixture of NB and R6G, rotated them from 240 to 130 rpm at 18 to 14 V, 50 kHz, and collected the time-dependent Raman signals of both analytes. As each type of molecule has its unique Raman spectrum, the chemistry as well as the concentration of each analyte on the surface of nanomotors can be determined simultaneously (Figure 5 a–c). By employing the same fitting method used for the single
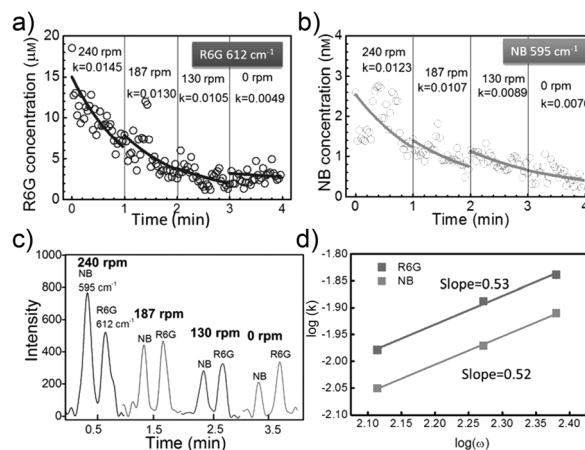

Figure 5. Tunable release of bi-analytes NB (a) and R6G (b) functionalized on the same nanomotor by the rotation speed. c) Representative Raman spectra of NB and R6G every 1 min at each rotation speed. d) The release rates of both analytes of NB and R6G, which monotonically increase with the rotation speed with a power-law dependence of 0.52 and 0.53, respectively.

chemical release, we determined the release rate k of each biochemical at different rotation speed ω. Both showed linear increment with ω with a power-law dependence of 0.52 and 0.53 for NB and R6G, respectively (Figure 5 d). The results demonstrated that the release of multiplex biochemicals has the dependence of $k \approx \omega^{0.5}$, same as that of single analyte release, which suggests that the model discussed before and used for single chemical release can be applied to understand the multiplex release. Moreover, we note that the release rate of NB ($k = 0.0076$–0.0123 s^{-1}) in the multiplex release system is consistently higher than that obtained as a single analyte ($k = 0.0017$–0.0044 s^{-1}). This could be attributed to the higher concentration and release rate of R6G molecules in the multiplex sample, where the dominating R6G could assist the detachment of NB molecules from the nanomotor sensors during its release and thus increased the release rate of NB.

Here, a much higher concentration of R6G is necessary in the mixed sample (R6G: ca. 20 μM, NB: a few nM) to obtain signals from both molecules on a similar level, which could be due to the much poorer attachment of R6G to AgNPs than that of NB.

In summary, we investigated a new mechanism for tuning the release rate of biochemicals from the surface of nanoparticles by controlled mechanical rotation. The investigation was carried out by both experimentation and analytic modeling. We synthesized, assembled, and rotated plasmonic nanomotors for this study. The kinetics of molecules release from the nanomotors was monitored by high-speed Raman spectroscopy. Both single and multiple analytes can be released at desirable rates by controlling the rotation speeds of nanomotors. The release rate shows a power-law dependence of approximately 0.5 with the rotation speed. The fundamental mechanism can be attributed to the convection-induced thickness reduction of the diffusion layer, which agrees with the experimental results quantitatively. To our best knowledge, such an effect is observed on micro/nano-scale devices for the first time. The nanomotor sensors could be potentially interesting for various biologically relevant applications, such as tunable biochemical release in an in vitro setting, although great efforts should be spent to work out the technical details and demonstrations. This research could potentially inspire a new form of device for robotized SERS sensors.

[1] T. L. Doane, C. Burda, *Chem. Soc. Rev.* **2012**, *41*, 2885–2991.
[2] a) R. Bardhan, W. Chen, M. Bartels, C. Perez-Torres, M. F. Botero, R. W. McAninch, A. Contreras, R. Schiff, R. G. Pautler, N. J. Halas, A. Joshi, *Nano Lett.* **2010**, *10*, 4920–4928; b) M.-R. Choi, K. J. Stanton-Maxey, J. K. Stanley, C. S. Levin, R. Bardhan, D. Akin, S. Badve, J. Sturgis, J. P. Robinson, R. Bashir, N. J. Halas, S. E. Clare, *Nano Lett.* **2007**, *7*, 3759–3765.
[3] X. Xu, H. Li, D. Hasan, R. S. Ruoff, A. X. Wang, D. L. Fan, *Adv. Funct. Mater.* **2013**, *23*, 4332–4338.
[4] D. Fan, Z. Yin, R. Cheong, F. Q. Zhu, R. C. Cammarata, C. L. Chien, A. Levchenko, *Nat. Nanotechnol.* **2010**, *5*, 545–551.
[5] Z. P. Xu, Q. H. Zeng, G. Q. Lu, A. B. Yu, *Chem. Eng. Sci.* **2006**, *61*, 1027–1040.
[6] J. Orozco, D. Vilela, G. Valdés-Ramírez, Y. Fedorak, A. Escarpa, R. Vazquez-Duhalt, J. Wang, *Chem. Eur. J.* **2014**, *20*, 2866–2871.
[7] A. K. Salem, P. C. Searson, K. W. Leong, *Nat. Mater.* **2003**, *2*, 668–671.
[8] a) B. Wildt, D. Wirtz, P. C. Searson, *Nat. Protoc.* **2010**, *5*, 1273–1280; b) P. Mali, N. Bhattacharjee, P. C. Searson, *Nano Lett.* **2006**, *6*, 1250–1253.
[9] S. E. Lee, G. L. Liu, F. Kim, L. P. Lee, *Nano Lett.* **2009**, *9*, 562–570.
[10] P. M. Peiris, L. Bauer, R. Toy, E. Tran, J. Pansky, E. Doolittle, E. Schmidt, E. Hayden, A. Mayer, R. A. Keri, M. A. Griswold, E. Karathanasis, *ACS Nano* **2012**, *6*, 4157–4168.
[11] L. Soler, V. Magdanz, V. M. Fomin, S. Sanchez, O. G. Schmidt, *ACS Nano* **2013**, *7*, 9611–9620.
[12] W. Wang, S. Li, L. Mair, S. Ahmed, T. J. Huang, T. E. Mallouk, *Angew. Chem. Int. Ed.* **2014**, *53*, 3201–3204; *Angew. Chem.* **2014**, *126*, 3265–3268.
[13] K. Kim, X. Xu, J. Guo, D. L. Fan, *Nat. Commun.* **2014**, *5*, 3632.
[14] a) D. L. Fan, F. Q. Zhu, R. C. Cammarata, C. L. Chien, *Nano Today* **2011**, *6*, 339–354; b) D. Fan, F. Zhu, R. Cammarata, C. Chien, *Phys. Rev. Lett.* **2005**, *94*, 247208; c) D. L. Fan, F. Q. Zhu, R. C. Cammarata, C. L. Chien, *Appl. Phys. Lett.* **2004**, *85*, 4175–4177.
[15] a) A. Campion, P. Kambhampati, *Chem. Soc. Rev.* **1998**, *27*, 241–250; b) X. B. Xu, K. Kim, H. F. Li, D. L. Fan, *Adv. Mater.* **2012**, *24*, 5457–5463.
[16] a) E. Klipp, W. Liebermeister, C. Wierling, A. Kowald, H. Lehrach, R. Herwig, *Systems Biology*, Wiley-Blackwell, Oxford, **2009**; b) J. L. Arlett, E. B. Myers, M. L. Roukes, *Nat. Nanotechnol.* **2011**, *6*, 203–215.
[17] G. Férey, *Chem. Soc. Rev.* **2008**, *37*, 191–214.
[18] a) K. J. Lee, P. D. Nallathamby, L. M. Browning, C. J. Osgood, X.-H. N. Xu, *ACS Nano* **2007**, *1*, 133–143; b) C. Greulich, S. Kittler, M. Epple, M. Köller, *Langenbecks Arch Surg.* **2009**, *38*, 11–13; c) M. E. Samberg, E. G. Loboa, S. J. Oldenburg, N. A. Monteiro-Riviere, *Nanomedicine* **2012**, *7*, 1197–1209; d) J.-J. Lin, W.-C. Lin, S.-D. Li, C.-Y. Lin, S.-h. Hsu, *ACS Appl. Mater. Interfaces* **2013**, *5*, 433–443; e) L. Pauksch, S. Hartmann, M. Rohnke, G. Szalay, V. Alt, R. Schnettler, K. S. Lips, *Acta Biomater.* **2014**, *10*, 439–449.
[19] V. Amendola, O. M. Bakr, F. Stellacci, *Plasmonics* **2010**, *5*, 85–97.
[20] T. M. Whitney, P. C. Searson, J. S. Jiang, C. L. Chien, *Science* **1993**, *261*, 1316–1319.
[21] a) D. K. Yi, S. T. Selvan, S. S. Lee, G. C. Papaefthymiou, D. Kundaliya, J. Y. Ying, *J. Am. Chem. Soc.* **2005**, *127*, 4990–4991; b) C. Graf, D. L. J. Vossen, A. Imhof, A. van Blaaderen, *Langmuir* **2003**, *19*, 6693–6700.
[22] K. A. Willets, R. P. Van Duyne, *Annu. Rev. Phys. Chem.* **2007**, *58*, 267–297.
[23] a) M. Hu, F. S. Ou, W. Wu, I. Naumov, X. Li, A. M. Bratkovsky, R. S. Williams, Z. Li, *J. Am. Chem. Soc.* **2010**, *132*, 12820–12822; b) M. S. Schmidt, J. Hübner, A. Boisen, *Adv. Mater.* **2012**, *24*, OP11–OP18.
[24] a) E. C. Le Ru, P. G. Etchegoin, *Annu. Rev. Phys. Chem.* **2012**, *63*, 65–87; b) E. J. Blackie, E. C. Le Ru, P. G. Etchegoin, *J. Am. Chem. Soc.* **2009**, *131*, 14466–14472.
[25] E. C. Le Ru, E. Blackie, M. Meyer, P. G. Etchegoin, *J. Phys. Chem. C* **2007**, *111*, 13794–13803.
[26] D. L. Fan, R. C. Cammarata, C. L. Chien, *Appl. Phys. Lett.* **2008**, *92*, 093115.
[27] a) D. L. Fan, F. Q. Zhu, X. Xu, R. C. Cammarata, C. L. Chien, *Proc. Natl. Acad. Sci. USA* **2012**, *109*, 9309–9313; b) T. B. Jones, *Electromechanics of Particles*, Cambridge University Press, New York, **1995**.
[28] A. J. Brad, L. R. Faulkner, *Electrochemical Methods*, Wiley, New York, **1980**.
[29] B. R. Munson, D. F. Young, T. H. Okiishi, *Fundamentals of Fluid Mechanics*, 4th ed., Wiley, Hoboken, **2002**.
[30] a) J. Nikolic, E. Expósito, J. Iniesta, J. González-Garcia, V. Montiel, *J. Chem. Educ.* **2000**, *77*, 1191–1194; b) V. G. Levich, *Physicochemical Hydrodynamics*, Prentice-Hall, New York, **1962**.